Fault-Tolerant Capability Analysis of Six-Phase Induction Motor with Distributed, Concentrated and Pseudo-Concentrated Windings

M. Alemi-Rostami[a], G. Rezazadeh[b,*], F. Tahami[b], H. R. Akbari-Resketi[c]

[a] Department of Electrical Engineering, Khayam Research Institute (KRI), Ministry of Science, Research, and Technology, Tehran, Iran.
[b] Department of Electrical Engineering, Sharif University of Technology, Tehran, Iran.
[c] Department of Electrical and Computer Engineering, Babol Noshirvani University of Technology, Babol, Iran.

[*] Corresponding author: Ghasem Rezazadeh, E-mail: S.g.rezazadeh.s@gmail.com, Tel: (+98)9111194112.

***Abstract*—Six-phase motors are becoming more popular because of their advantages such as lower torque ripple, better power distribution per phase, higher efficiency, and fault-tolerant capability compared to the three-phase ones. This paper presents the fault-tolerant capability analysis of a symmetrical six-phase induction motor equipped with distributed, conventional concentrated, and pseudo-concentrated windings under open-circuit fault scenarios. For further investigation, different load types such as constant-speed, constant-torque, and constant-power are applied to the motor. Two concepts of magnetic and physical phase separations are introduced as factors affecting the motor reliability. Analytically, these factors give an insight into how the pseudo-concentrated winding could be a fault-tolerant alternative. Moreover, five parameters such as the change of output power, power loss, power factor, efficiency, and expected load loss are considered as the fault-tolerant capability parameters to evaluate the windings' reliability. The aforementioned parameters are reported using the finite element analysis for different fault scenarios and different load types. Although the baseline motor dimensions are not optimized for applying the pseudo-concentrated winding, the pseudo-concentrated shows a promising performance with high fault-tolerant capability.**

***Index Terms*—**Concentrated winding, Distributed winding, Expected load loss, Fault-tolerant capability, Magnetic separation, Open-circuit fault, Pseudo-concentrated winding, Physical phase separation, Reliability analysis, Six-phase induction machine.

1. INTRODUCTION

In recent years, multi-phase motors have been an attractive option in several applications such as electric vehicle and railway traction, all-electric ships, and more-electric aircraft [1]. The multi-phase motors have several advantages over their three-phase counterpart: One of them is splitting the power into multiple phases to reduce the power ratings per phase. Another one is improving the distribution of the magneto motive force in the motor air gap, thereby reducing torque ripples [2]. In addition, the degrees of freedom are increased with the number of independent phase variables of the driver, which helps optimizing the control strategies [3]. One of the most advantages of these motors is their high fault-tolerant capability [4], which results in being used for sensitive applications with high required reliability. Among the numerous possibilities of the multiphase motors, the six-phase induction motor (6PIM) is one of the most frequently used multiphase motors due to the simplicity of its structure identical with three-phase motor from air gap point of view [5].

Several papers have focused on the structure of the 6PIM in healthy conditions and tried to improve the motor performance parameters [6]-[9]. Some other papers studied the post-fault operation of 6PIM under open-phase or short-circuited phase conditions [10]-[14]. Also, several research is focused on the modelling [5], [15], [16] and control aspects [1], [17]-[19] at post fault condition. However, there is no comprehensive fault-tolerant capability analysis for different winding configurations. This paper discusses the fault tolerant capability of the 6PIM equipped with different winding configurations (such as distributed, concentrated, and pseudo-concentrated windings) under different fault scenarios.

Recently, many valuable published works focused on the reliability evaluation of electrical machines [20]-[24]. Various studies on motor reliability have shown that about 30% to 40% of induction motor failures are caused by stator winding faults [25]-[26]. This fault is due to dynamic load conditions or a combination of different stresses acting on stator winding such as thermal or electrical stresses [27]. Among the possible faults related to the stator windings, open circuit fault (OCF) of stator windings is a common problem [25] and will be discussed here.

In this paper, the performance parameters of the 6PIM equipped with the distributed winding (DW), concentrated winding (CW), and pseudo-CW under different OCF scenarios are examined. In addition, different load types such as constant-speed, constant-torque, and constant-power are employed to study their effects on the motor's reliability. As an analytical approach, two concepts of magnetic and physical phase separations are used, which are closely related to the motor's reliability. Using

these concepts can give an insight into how the pseudo-CW could be a fault-tolerant alternative. To more accurately examine the windings' fault tolerant capability, the changes of five parameters (output power, power loss, power factor, efficiency, and expected load loss) are investigated. The finite element analysis is used to calculate the aforementioned parameters under different fault scenarios and different load types. The reliability analysis shows that the pseudo-CW has satisfying fault tolerant capability close to the DW and much higher than the CW. It should be noted that the baseline motor is not optimized for applying the pseudo-CW and CW.

The paper structure is organized as follows: the configuration of the baseline 6PIM equipped with DW, CW, and pseudo-CW and their performance characteristics are presented in section 2. The magnetic and physical separation concepts and different possible fault scenarios are explained in section 3. The motor performance in post fault conditions is discussed in section 4. Section 5 presents a comparison between the considered winding layouts from the reliability point of view. Subsequently, a conclusion is presented based on the reported discussions and results.

2. Baseline 6PIM performance

The induction motor with the 24-slot stator and squirrel-cage 18-bar rotor cores is considered as the baseline motor. The main geometrical dimensions of the baseline motor are shown in Table 1. Three different two-pole symmetrical six-phase winding configurations (with 60^o phase shift angle between each phase and its nearest phases) are applied to the baseline 6PIM including: one-layer DW, two-layer conventional CW, and four-layer pseudo-CW (see Figure 1). The performance parameters of the 6PIM equipped with the aforementioned winding layouts are reported in Table 2.

2.1 One-Layer Distributed Winding

The one-layer distributed winding layout is shown in Figure 1 (a). By connecting the motor to the power supply (14 V), simulation results of the finite element analysis (FEA) and experimental results have been reported in Table 2. According to the simulation results, the no-load current is 1.45 A and the full-load current is 1.82 A. In comparison, the experimental results show 1.41 A and 1.78 A for the no-load and full-load currents, respectively. Moreover, FEA simulation results show that the rotor rated speed and torque are 2822 rpm and 0.3 N.m, respectively. It should be noted that measured values are 2820 rpm and 0.3 N.m, respectively.

2.2 Two-Layer Concentrated Winding

The two-layer concentrated winding layout is shown in Figure 1 (b). As shown in Table 2, the conventional two-layer CW for 6PIM does not have proper performance compared to the other winding layouts because of its low-quality air gap flux density distribution. FEA results show that the conventional two-layer CW has much lower output power compared to the DW on the same rotor speed. The conventional CW in comparison to DW has shorter end-winding which results in a less copper usage, smaller resistance and consequently fewer copper losses [7]. However, the CW efficiency is lower than the DW because of its low output power value.

2.3 Four-Layer Pseudo–Concentrated Winding

The pseudo-CW (see Figure 1 (c)) layout benefits from the advantages of the CW and has a higher fundamental harmonic amplitude of air gap flux density with lower THD compared to the CW. The performance characteristics of the pseudo-CW is not as good as DW, but they are much higher than that of the CW. Considering the FEA results, the motor has 1.78 A full-load current, 2820 rpm rated speed, and 0.151 N.m rated torque. In comparison, the experiment has reported 1.8 A, 2820 rpm, and 0.16 N.m, respectively.

3. Magnetic and physical phase separations

3.1 Physical phase separation

The motor hot spot is usually placed in the stator slots where the major heat source (conductive loss) cannot be dissipated easily and causes damage to the insulation winding [28]. The stator winding faults are generally related to the insulation failure. This fault starts as an undetected turn-turn fault and finally grow and culminate into phase-phase faults [25]. One of the winding features that can prevent the initiation of the phase-phase faults is the physical phase separation between different phases. The most complete type of physical separation occurs when only one coil is placed in each slot (using single-layer configuration) and no overlapping between different phases occurs in the end winding. For example, in single-layer DW configuration, there is overlapping in the end-winding region. Therefore, among the different winding types, the single-layer CW (winding on tooth) has the most physical separation between different phases.

As shown in Figure 1 (a), in the end-winding region of the DW, phase A_1 is in contact with all phases except phase B_2, because in the short-pitch DW configuration each phase is not in contact with its opposite phase. Otherwise, in the conventional full-pitch DW, each phase is in contact with all the other phases and somehow forms a bulky end-winding. On the other hand, the produced heat by winding conductive loss could be trapped in bulky end winding part causing a heat transferring problem. From an analytical point of view, the physical phase separation of the DW configuration is not acceptable at all.
In CW configuration, each phase is in contact with two other phases in the slots because of its two-layer configuration and no winding overlap is seen in the end winding part. In the considered four-layer pseudo-CW, each phase is in contact with three other phases in the stator slots and no overlap between different phases occurs in the end winding part [6].
It should be noted that the baseline 6PIM is not optimized for applying pseudo-CW and its dimensions were designed for DW application. In [6], which 6PIMs performance parameters are reported in the healthy condition, the four-layer pseudo-CW is proposed for the first time to achieve higher performance parameters compared to CW. Since only the performance results of the four-layer pseudo-CW were available, eventually they were compared with the single-layer DW and the two-layer CW. Considering the physical separation results, the pseudo-CW has satisfying condition better than DW.

3.2 Magnetic separation

Beside the physical phase separation, magnetic separation between different phases is an important parameter to enhance the fault tolerant capability [29]. Without magnetic isolation, fault in one phase can induce voltages in other phases. Thus, the motor should be designed with minimal mutual coupling between different phases. In other words, a zero mutual inductance between phases and high self-inductance for each phase are the most suitable magnetic characteristic for the motor considering the reliability aspect, because these features prevent spreading the fault from one phase to the another magnetically.
The ratio of the mutual inductance between the different phases to the self-inductance of the phase is considered as an index to measure a motor's fault tolerant capability. This ratio should be close to zero in an ideal condition where the phases will be fully separated magnetically [30]. It should be noted that this ratio is not a novel parameter to investigate the fault tolerant capability such that its concept is reported in [30] and its related calculations are presented in [31]. The inductances ratio for the fault-tolerant capability between phase *x* and phase *y* is:

$$IRFT_{xy} = \frac{L_{xy}}{L_{xx}} \tag{1}$$

Assuming that the air gap length is a constant value for whole spatial angels (φ), the mutual inductance between phases *x* and *y* would be [31]:

$$L_{xy} = \frac{\psi_{xy}}{i_x} = \frac{\mu_0 R l}{g} \int_0^{2\pi} N_x(\varphi) TF_y(\varphi) d\varphi \tag{2}$$

In equation (2), ψ_{xy} is the mutual flux linkage between phases *x* and *y* and TF_x is the turn function of the phase *x*. The self-inductance of phase *x* is [31]:

$$L_{xx} = \frac{\mu_0 R l}{g} \int_0^{2\pi} N_x(\varphi) TF_x(\varphi) d\varphi \tag{3}$$

For the pseudo-CW, this ratio is equal to 0.227 between phase A_1 and other phases except for phase B_2. Phase B_2 is a redundant phase of phase A_1 and has similar configuration to phase A_1 with opposite direction of current fellow so it is obvious that this phase has a strong magnetic coupling to the phase A_1 ($IRFT_{A1B2}$=1). According to the results, the pseudo-CW ($IRFT_{Pseudo\text{-}CW}$=0.227) has more separated phases magnetically than DW ($IRFT_{DW}$=0.423) and less than CW ($IRFT_{CW}$=0). Therefore, even if the baseline motor dimensions are not optimized for the pseudo-CW, the results were satisfying. The FEA results for the phases inductance matrix are reported in Table 3. As can be seen, the FEA results completely validate the accuracy of the obtained analytical results considering phase-to-phase inductance, phase self-inductances, and *IRFT* values. It should be noted that the little difference between the analytical and FEA results comes from the fact that FEA takes more magnetic aspects into account such as slotting effect, core nonlinear magnetic behavior, and coil leg placement in slot layers.

4. Faulty and healthy conditions report using FEA

The six-phase motor has the ability to operate in OCF condition, where up to 3 phases are lost. As shown in Figure 2, Five different OCF types, which could occur in the six-phase motor and the motor still continue to produce torque, are one-phase

(IPh), adjacent double-phase (A2Ph), non-adjacent double-phase (NA2Ph), adjacent triple-phase (A3Ph), and non-adjacent triple-phase (NA3Ph) fault. Table 4 presents the fault scenarios considering seven possible open-circuit faults. These scenarios were considered to be studied on the 6PIM equipped with the DW, CW, and pseudo-CW. It should be noted that each explained fault scenario occurs with six different combinations with different phases involved.

The motor is simulated in healthy and faulty conditions using the finite element analysis. The FEA results are obtained by using a time-transient simulation in 2D Ansys Maxwell software. The flux density distribution of the 6PIM equipped with the DW under healthy and two-phase fault condition are shown in Figure 3. In the same way, the flux density distributions of the 6PIM equipped with the CW and pseudo-CW are shown in Figure 4 and Figure 5, respectively. As can be seen, when the OCF occurs the flux density amplitude is reduced especially in the stator and rotor teeth. Because the phase currents are the source of producing flux in the stator and rotor magnetic path, the flux density amplitude surely will be decreased without some of these flux producing sources (by OCF occurrence). In Figure 6, the phase current under 2A OCF scenario is shown for different winding types. The presence of current harmonics is evident and results in higher output torque ripple. The FEA simulation results of 6PIM equipped with DW, CW and pseudo-CW under different scenarios are reported in Table 5 to Table 7. The results were obtained using three different load types such as constant-speed, constant-torque, and constant-power to consider the load type effects on the motor fault tolerant capability.

The obtained results show that when an OCF occurs, the current in the adjacent phase is increased to compensate for the reduced MMF. In other words, if one or more phases are lost, the current of healthy phases increases to maintain the power of the motor. In this situation, the power losses of the remaining phases are increased and consequently the windings could be damaged. For this reason, a power derating factor is required to keep the windings safe. It should be noted that as the number of phase-fault increases, the amount of derating factor will increase. Therefore, spreading the fault from one phase to another has a great impact on the derating factor in post-fault condition. Therefore, more phase physical and magnetic separation could help to reduce the load loss amount in post-fault condition. As can be seen in Table 4, during 1A scenario, the current flows through the stator is increased by 1.2 times in phases A_2 and B_1 and 1.3 times in phase B_2 and 1.14 times in phase C_1 and C_2 approximately for the 6PIM equipped with DW using the constant-speed load compared to the healthy condition.

It should be noted that the conventional CW (applied to the baseline 6PIM) doesn't have proper performance parameters even in healthy condition and the winding performance gets worse in the post-fault conditions especially when the constant-power or constant-torque are applied. Therefore, the motor cannot produce enough power to rotate the load. Therefore, to have reliable results for comparison and avoiding unjustified performance results, the FEA results for the performance of the 6PIM equipped with the CW are not reported in post-fault conditions when constant-power and constant-torque load types are applied to the motor because the motor cannot operate in these situations properly.

5. Fault tolerant analysis

5.1 Reliability

After presenting the motor performance parameters in post-fault conditions, these parameters could be used in a reliability analysis to investigate the fault tolerant capability of the 6PIM equipped with the DW, CW, and pseudo-CW. To use this analysis method, first some fundamental aspects of the reliability analysis should be explained here. Reliability is the probability of performing adequately to achieve the desired aim of the system in a specified time [32].

One of the useful reliability indices to evaluate the motor fault tolerant capability is the Expected Load Loss (ELL), which indicates the expected amount of load cannot be supplied in post-fault condition considering the fault occurrence probability [33]. The ELL can be calculated as [34]:

$$ELL = \sum_{i=1}^{n} (PLL) \times P_{LL} \tag{4}$$

As can be seen, the ELL value depends on probability of load loss (*PLL*) and the load loss amount (P_{LL}). Before proceeding to the probability part of the reliability analysis (*PLL* calculation), it is necessary to express the utilized assumptions for the reliability analysis. To simplify the reliability analysis procedure, some assumptions are used as follows:

1) The probability of losing each phase is equal to *Q(t)*, which is a function of time.
2) The fault occurrence in each phase is independent to the operation conditions of other phases. In other words, fault occurrence in phases is an independent probability event.

Now, it is necessary to calculate the *Q(t)* for fault occurrence in each phase. Considering the reliability concept, the probability of a component (winding phase) surviving for a time *t* with a constant failure rate of λ is [22]:

$$P(t) = e^{-\lambda t} \tag{5}$$

Therefore, the probability of fault occurrence in each phase can be described as:

$$Q(t) = 1 - P(t) = 1 - e^{-\lambda t} \tag{6}$$

An example for calculating the (P_{LL}) for the OCF scenario where A_1 and B_1 are the faulty phases, could clarify how (P_{LL}) value is related to the *P(t)* and *Q(t)*. In this scenario, four components are up and two components are down so the probability is:

$$P(faulty\ \ phases : A_1 \& B_1) = P^4(t)Q^2(t) = e^{-4\lambda t}(1 - e^{-\lambda t})^2 \tag{7}$$

It should be noted that there are many OCF scenarios for each case study; therefore, the ELL formula for each case study (6PIM with each winding configuration) is too long. Thus, the obtained ELL equations of the case studies are not reported in this paper for the sake of brevity.

The failure rate of the 6PIM phase winding is equal to 15×10^{-8} [22]. Using the presented equations and utilized failure rate, the ELL values for the 6PIM equipped with different winding configurations are calculated after one million hours and will be discussed in the next section. It should be noted that for ELL calculation the FEA simulation results are used for the amount of load loss.

5.2 Results & discussion

The effect of OCF occurrence on five performance parameters such as the output power, power loss, power factor, efficiency, and expected load loss are investigated to evaluate the windings reliability. These parameters are carefully studied using the FEA results as follows:

1) Output power: Figure 7 shows the output power of the 6PIM equipped with DW, CW, and pseudo-CW in different fault scenarios with different load types. In constant-torque and constant-power load types, the change in output power is negligible because the loads demand almost constant output power. Considering this fact, the best load type to study the effect of fault occurrence on output power is the constant-speed one. In constant-speed load, the normalized output powers of the 6PIM equipped with the pseudo-CW are very close to the ones of the 6PIM with the DW in different scenarios. Even in 1A and 3C scenarios, the output power reduction of the pseudo-CW is less than that of the DW.

However, the output power variation of the CW in different OCF scenarios, show an unacceptable fault tolerant capability for the CW, even if the CW has the highest phase separation compared to the DW and pseudo-CW. The main reason is the fact that even in healthy condition, the CW does not have proper performance parameters and it is not a suitable winding configuration for IM application. On the other hand, the pseudo-CW has satisfying fault tolerant capability considering the output power reduction compared to the DW.

To investigate the windings output power in faulty conditions even more, Figure 8 shows the minimum and average output powers for the 6PIM equipped with the DW, CW, and pseudo-CW when different load types are applied to the motor. As can be seen once more, the pseudo-CW provides similar minimum and average output power close to the DW in post-fault conditions.

2) Power loss: Figure 9 shows the normalized power loss of the 6PIM equipped with the considered winding layouts. Considering these results, it is clear that the motor power loss is increased after fault occurrence as it was expected. However, the pseudo-CW has the power loss growth higher than the CW and fortunately lower than the DW. Therefore, the pseudo-CW has better fault tolerant capability compared to the DW considering the power loss growth factor.

For further investigation, Figure 10 shows the minimum and average power loss for the 6PIM equipped with the DW, CW, and pseudo-CW when different load types are applied to the motor. Clearly, the power loss growth in case of using the pseudo-CW is lower than the one with DW.

3) Efficiency: as mentioned many times, the baseline 6PIM laminations are designed to apply DW, thus, the DW has the best efficiency in healthy condition. By reporting the absolute value of the efficiency for different winding configurations, the DW will have the highest efficiency values in every fault scenario because of its superior performance in the designed laminations. However, the aim of this paper is only to discuss the effect of the OCF occurrence on different windings to evaluate their fault tolerant capability; therefore, instead of reporting the absolute value of the windings' efficiency, their efficiency regulation value compared to their healthy condition will be reported as follows:

$$\eta\, regulation(\%) = \frac{\eta_{healthy} - \eta_{mutual}}{\eta_{healthy}} \times 100 \quad (8)$$

This way, the change in the efficiency value caused by the fault occurrence can be observed easily. Figure 11 shows the efficiency regulation for the 6PIM equipped with the considered winding layouts. As can be seen, the pseudo-CW has similar changes of the efficiency value as DW. However, the CW doesn't have an acceptable behavior compared to the other winding layouts. It can be stated that considering the efficiency parameter, the pseudo-CW and DW are the layouts with satisfying fault tolerant capability.

4) Power factor: the power factor changes are investigated with the same scenario as the one was employed for the efficiency. In other words, the power factor regulation is chosen to be studied instead of actual absolute value of the power factor:

$$PF\ regulation(\%) = \frac{PF_{healthy} - PF_{mutual}}{PF_{healthy}} \times 100 \quad (9)$$

As shown in Figure 12, the pseudo-CW has the higher fault tolerant capability compared to the CW and DW considering the reported power factor variation in different load types and OCF scenarios.

5) Expected load loss: using the reliability analysis presented in the previous section, the expected load loss values for the 6PIM equipped with the DW, pseudo-CW, and CW are calculated in different load types. The obtained ELL equations are functions of time with long length; therefore, to make it possible to compare the windings' ELL values, the ELL values are reported after one million hours and using the phase failure rate of 15×10^{-8}. The calculated ELL results are reported in Figure 13. As can be seen, the pseudo-CW has approximately 46%, 31%, and 8% lower ELL values compared to the DW in constant-speed, constant-torque, and constant-power load types, respectively. In addition, it has 37% lower ELL value compared to the CW in constant-speed load type. Therefore, it can be concluded that considering all the five reliability parameters especially the ELL, the pseudo-CW has the highest fault tolerant capability compared to the CW and DW. It should be noted that the fault tolerant capability of the pseudo-CW could be enhanced even more with a proper redesign of the 6PIM dimensions [10].

6. Conclusion

This paper presented the fault tolerant capability analysis of the 6PIM equipped with the DW, CW and pseudo-CW under different OCFs scenarios (loosing up to three phases) and different load types (constant-speed, constant-power, and constant-torque). Two concepts of magnetic and physical phase separations were considered, which have impact on motor's reliability. The results showed that the CW has the best and DW has the worst phase separation magnetically and physically.

To continue analyzing the windings' fault tolerant capability, five parameters such as efficiency, power factor, output power, power loss, and expected load loss were studied in post-fault condition to monitor the windings behavior after fault occurrence. Investigating these parameters showed that the pseudo-CW has higher fault tolerant capability compared to the DW and CW with much lower (from 8% to 53%) ELL values in different load types. It should be mentioned that the pseudo-CW was applied to the 6PIM laminations designed for applying DW; therefore, by designing a completely new motor compatible with the pseudo-CW features, the motor performance and consequently its fault tolerant capability could be enhanced.

It can be concluded that although the CW has the highest phase separation, it hasn't acceptable fault tolerant capability compared to DW and pseudo-CW. The main reason is the fact that even in healthy condition, the CW does not have proper performance parameters and it is not a suitable winding configuration for 6PIM application.

REFERENCES

1. Baneira, F., Doval-Gandoy, J., Yepes, A.G., et al. "Comparison of postfault control strategies in terms of converter losses for dual three-phase machines", *IEEE Energy Conversion Congress and Exposition (ECCE)*, pp. 3612-3619 (2017).
2. Abdel-Khalik, A.S., Hamad, M.S., Massoud A.M., et al. "Postfault operation of a nine-phase six-terminal induction machine under single open-line fault", *IEEE Transactions on Industrial Electronics*, **65**(2), pp. 1084-1096 (2017).
3. Salem, A. and Narimani, M. "A review on multiphase drives for automotive traction applications", *IEEE Transactions on Transportation Electrification*, **5**(4), pp. 1329-1348 (2019).
4. Baneira, F., Yepes, A.G., López, Ó., et al. "Estimation method of stator winding temperature for dual three-phase machines based on dc-signal injection", *IEEE Transactions on Power Electronics*, **31**(7), pp. 5141-5148 2015.

5. Kianinezhad, R., Nahid-Mobarakeh, B., Baghli, L., et al. "Modeling and control of six-phase symmetrical induction machine under fault condition due to open phases", *IEEE Transactions on Industrial Electronics*, **55**(5), pp. 1966-1977 (2008).
6. Rezazadeh, G., Tahami, F., Capolino, G.A., et al. "Improvement of concentrated winding layouts for six-phase squirrel cage induction motors", *IEEE Transactions on Energy Conversion*, **35**(4), pp. 1727-1735 (2020).
7. Rezazadeh, G., Vaschetto, S., Tahami, F., et al. "Analysis of six-phase induction motor with distributed and concentrated windings by using the winding function method", *XIII International Conference on Electrical Machines (ICEM)*, pp. 2423-2429 (2018).
8. Rezazadeh, G., Tahami, F., Capolino, G.A., et al. "Design of a Six-Phase Squirrel Cage Induction Motor with Pseudo-Concentrated Windings", *International Conference on Electrical Machines (ICEM)*, pp. 2097-2103 (2021).
9. Lin, C.H. and Hwang, C.C. "Multiobjective optimization design for a six-phase copper rotor induction motor mounted with a scroll compressor", *IEEE Transactions on Magnetics*, **52**(7), pp. 1-4 (2016).
10. Apsley, J. and Williamson, S. "Analysis of multiphase induction machines with winding faults", *IEEE Transactions on industry applications*, **42**(2), pp. 465-472 (2006).
11. Munim, W.N.W.A., Duran, M.J., Che, H.S., et al. "A unified analysis of the fault tolerance capability in six-phase induction motor drives", *IEEE Transactions on Power Electronics*, **32**(10), pp. 7824-7836 (2016).
12. Mule, G.J.A., Munim, W.N.W.A., Tousizadeh, M., et al. "Post-fault tolerant of symmetrical six-phase induction machine under open circuit fault with single and two isolated neutral points using graphical user interface", in *AIP Conference Proceedings*, p. 020016 (2019).
13. Salem, A. and Narimani, M. "Fault-Tolerant Operation of Asymmetrical Six-Phase Motor Drives in EV Applications", in *IEEE Transportation Electrification Conference & Expo (ITEC)*, pp. 210-215 (2020).
14. Alberti, L. and Bianchi, N. "Experimental tests of dual three-phase induction motor under faulty operating condition", *IEEE Transactions on Industrial Electronics*, **59**(5), pp. 2041-2048 (2011).
15. Pantea, A., Yazidi, A., Betin, F., et al. "Six-phase induction machine model for electrical fault simulation using the circuit-oriented method", *IEEE Transactions on Industrial Electronics*, **63**(1), pp. 494-503 (2015).
16. Chawla, R., Vinayak, B.A., and Jagadanand, G. "Modelling and detection of stator incipient open circuit fault in three-phase induction motor", in *IEEE International Conference on Power Electronics, Drives and Energy Systems (PEDES)*, pp. 1-6 (2018).
17. Duran, M.J. and Barrero, F. "Recent advances in the design, modeling, and control of multiphase machines—Part II", *IEEE Transactions on Industrial Electronics*, **63**(1), pp. 459-468 (2015).
18. Yepes, A.G., Doval-Gandoy, J., Baneira, F., et al. "Postfault strategy for dual three-phase machines with minimum loss in the full torque operation range under two open phases", in *IEEE Energy Conversion Congress and Exposition (ECCE)*, pp. 3380-3385 (2018).
19. Sala, G., Mengoni, M., Rizzoli, G., et al. "Impact of star connection layouts on the control of multiphase induction motor drives under open-phase fault", *IEEE Transactions on Power Electronics*, **36**(4), pp. 3717-3726 (2020).
20. Bramerdorfer, G. "Multiobjective electric machine optimization for highest reliability demands", *CES Transactions on Electrical Machines and Systems*, **4**(2), pp. 71-78 (2020).
21. Zagirnyak, M.V., Prus, V.V., Somka, O., et al. "Models of Reliability Prediction of Electric Machine Taking into Account the State of Major Structural Units", *Advances in electrical and electronic engineering*, **13**(5), pp. 71-78 (2015).
22. Li, W., and Cheng, M. "Investigation of influence of winding structure on reliability of permanent magnet machines", *CES Transactions on Electrical Machines and Systems*, **4**(2), pp. 87-95 (2020).
23. Giangrande P., Madonna, V., Nuzzo, S., et al. "Moving Toward a Reliability-Oriented Design Approach of Low-Voltage Electrical Machines by Including Insulation Thermal Aging Considerations", *IEEE Transactions on Transportation Electrification*, **6**(1), pp. 16-27 (2020).
24. Li, W., and Cheng, M. "Reliability Analysis and Evaluation for Flux-Switching Permanent Magnet Machine", *IEEE Transactions on Industrial Electronics*, **66**(3), pp. 1760-1769 (2019).
25. Nandi, S., Toliyat, H.A., and Li, X. "Condition monitoring and fault diagnosis of electrical motors—A review", *IEEE transactions on energy conversion*, **20**(4), pp. 719-729 (2005).

26. Kliman, G.B., Premerlani, W.J., Koegl, R.A., et al. "A new approach to on-line turn fault detection in AC motors", in *IAS'96. Conference Record of the 1996 IEEE Industry Applications Conference Thirty-First IAS Annual Meeting*, pp. 687-693 (1996).
27. Tavner, P.J. "Review of condition monitoring of rotating electrical machines", *IET electric power applications*, **2**(4), pp. 215-247 (2008).
28. Nategh, S., Krings, A., Wallmark, O., et al. "Evaluation of impregnation materials for thermal management of liquid-cooled electric machines", *IEEE Transactions on Industrial Electronics*, **61**(11), pp. 5956-5965 (2014).
29. Jack, A.G., Mecrow, B.C., and Haylock, J.A. "A comparative study of permanent magnet and switched reluctance motors for high-performance fault-tolerant applications", *IEEE transactions on industry applications*, **32**(4), pp. 889-895 (1996).
30. Alipour-Sarabi, R., Nasiri-Gheidari, Z., Tootoonchian, F., et al. "Analysis of Winding Configurations and Slot-Pole Combinations in Fractional-Slots Resolvers", *IEEE Sensors Journal*, **17**(14), pp. 4420-4428 (2017).
31. Toliyat, H.A., Nandi, S., Choi, S., et al. *"Electric Machines: Modeling, Condition Monitoring, and Fault Diagnosis"*, CRC Press (2017).
32. Kaboli, S. *"Reliability in power electronics and electrical machines: industrial applications and performance models: industrial applications and performance models*", IGI Global (2016).
33. Lin, J., Cheng, L., Chang, Y., et al. "Reliability based power systems planning and operation with wind power integration: A review to models, algorithms and applications", *Renewable and Sustainable Energy Reviews*, **31**(1), pp. 921-934 (2014).
34. Billinton, R. and Allan, R.N. *"Reliability evaluation of engineering systems"*, Springer (1992).

List of Figures:

List of Tables:

Table 3. FEA results for phase-to-phase inductances: (a) Distributed winding (b) Conventional concentrated winding (c) Pseudo-concentrated winding

Table 4. Different fault scenarios for symmetrical six-phase induction motor.

Table 5. FEA results for performance of 6PIM equipped with DW: (a) Constant-speed (b) Constant-torque (c) Constant-power

Table 6. FEA results for performance of 6PIM equipped CW: Constant-speed

Table 7. FEA results for performance of 6PIM equipped Pseudo-CW: (a) Constant-speed (b) Constant-torque (c) Constant-power

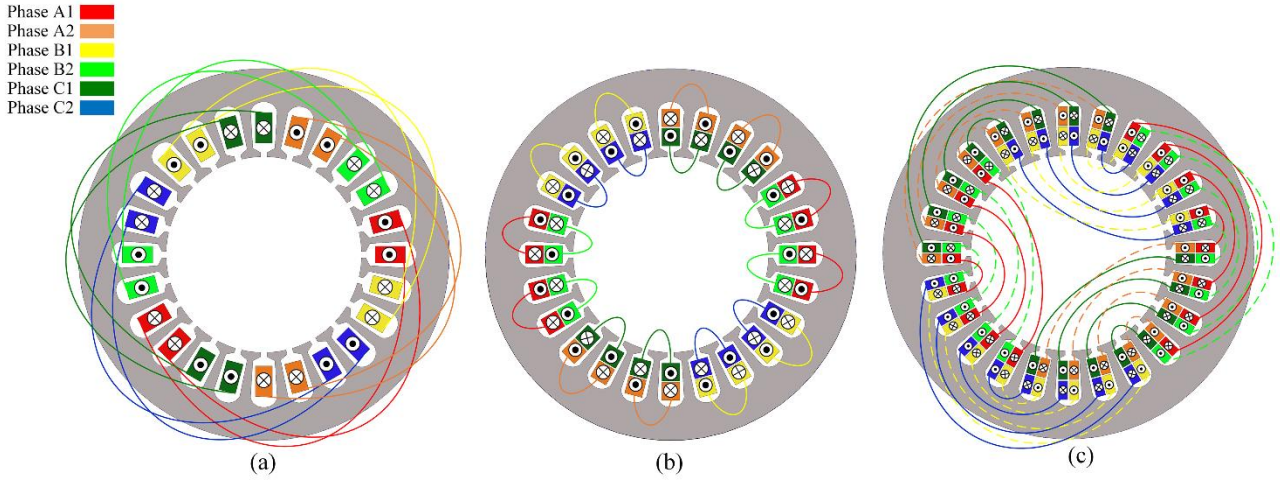

Figure 1. Two-pole winding layouts for the 6PIM: (a) Single-layer DW (b) Two-layer conventional CW (c) Four-layer pseudo-CW.

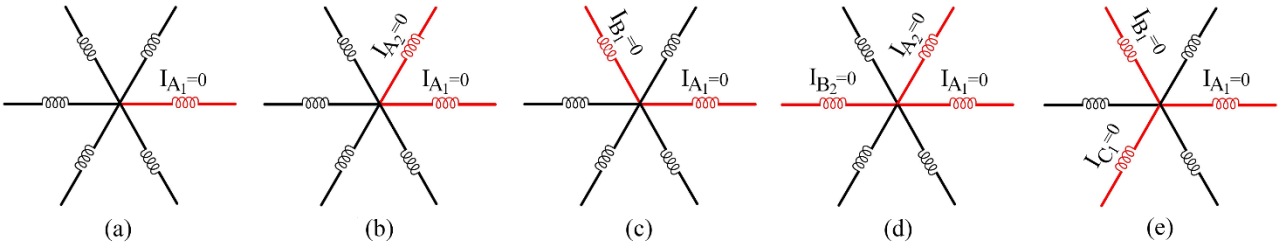

Figure 2. Open-circuit faults in phase windings of 6PIM: (a)1Ph (b)A2Ph (c)NA2Ph (d) A3Ph (e)NA3Ph.

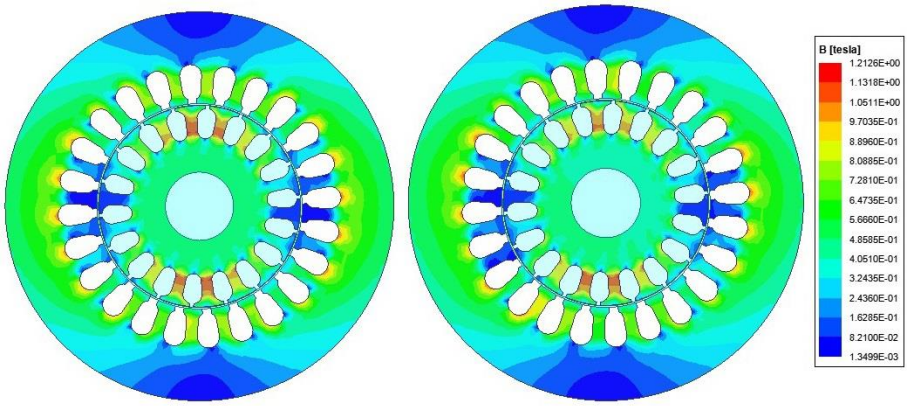

Figure 3. FEA results for flux density distribution of DW: (a) Healthy condition and (b) 2A OCF scenario

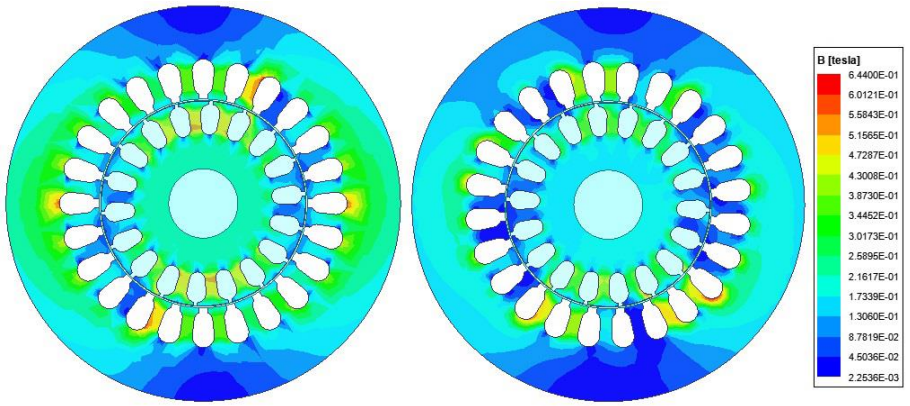

Figure 4. FEA results for flux density distribution of CW: (a) Healthy condition and (b) 2A OCF scenario

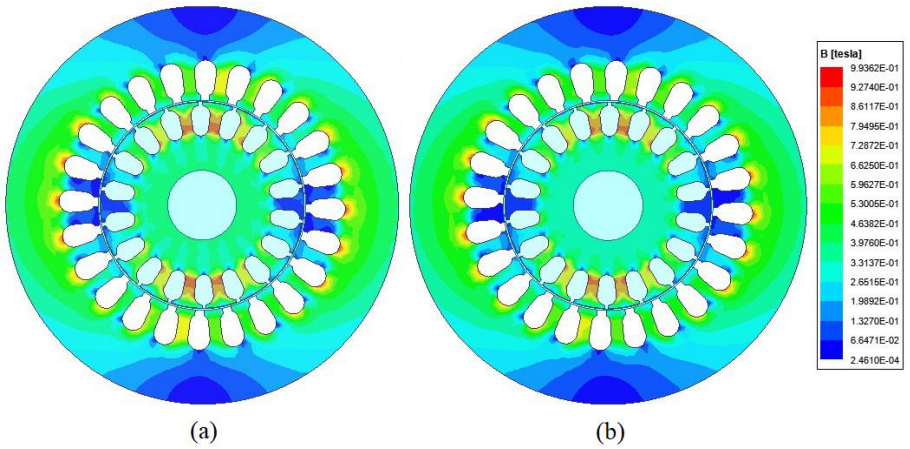

Figure 5. FEA results for flux density distribution of pseudo-CW: (a) Healthy condition and (b) 2A OCF scenario

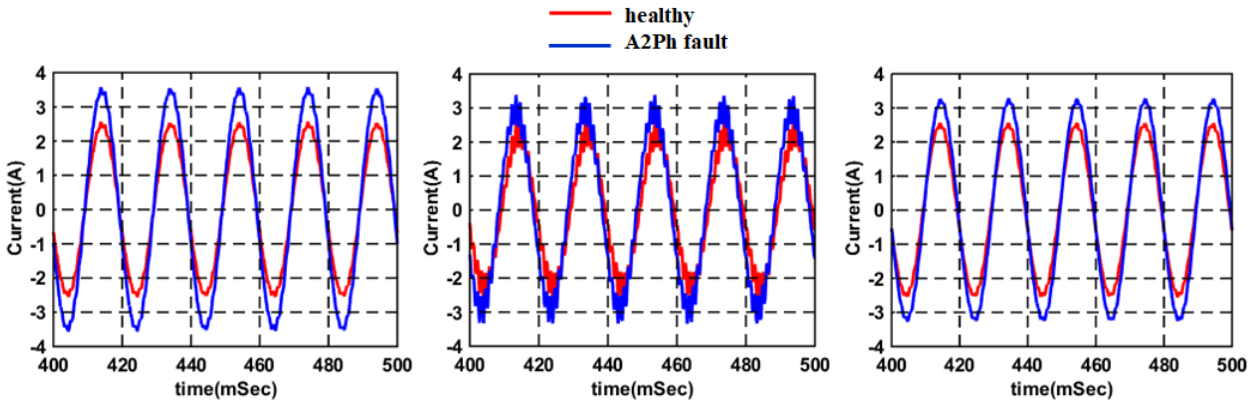

Figure 6. Phase current waveforms in healthy and faulty conditions: (a) DW (b) CW and (c) pseudo-CW.

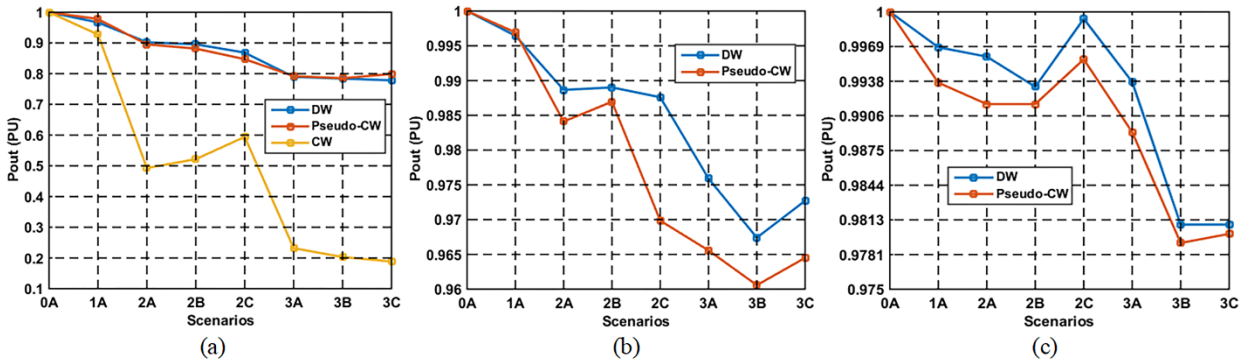

Figure 7. Output power of 6PIM under different fault scenarios: (a) Constant-speed (b) Constant-torque (c) Constant-power load types

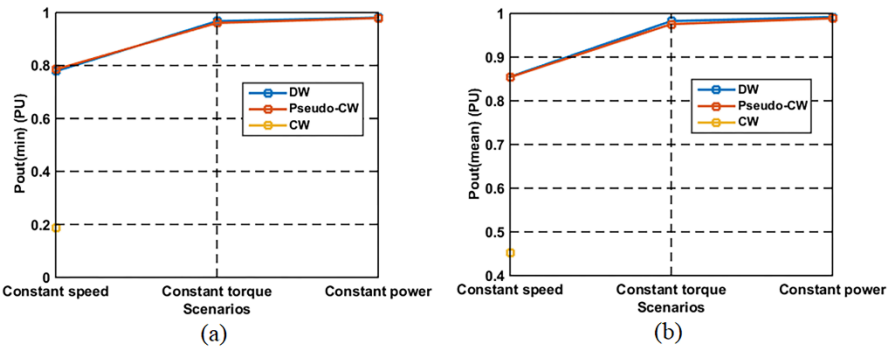

Figure 8. FEA results for (a) minimum and (b) average normalized output powers of 6PIMs with DW, CW, and pseudo-CW.

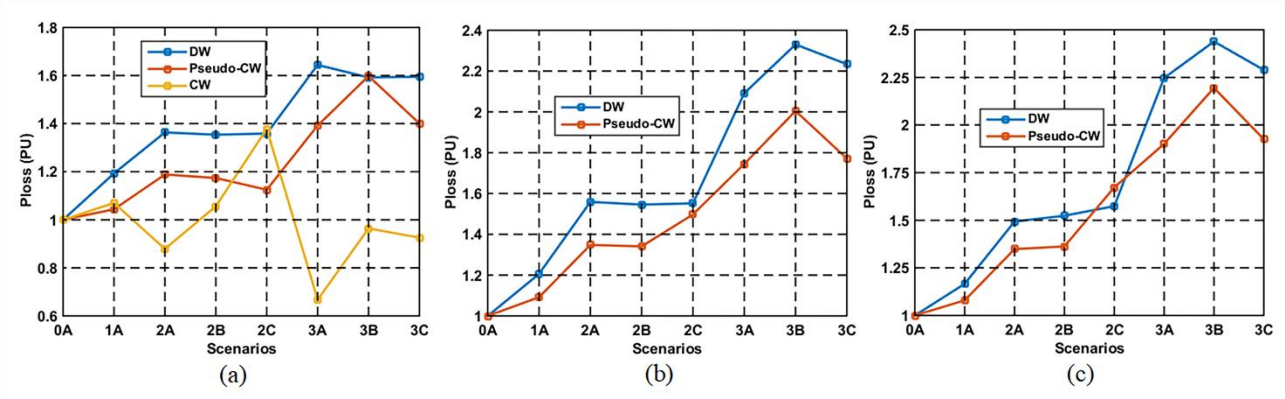

Figure 9. Power loss of 6PIM under different fault scenarios: (a) Constant-speed (b) Constant-torque (c) Constant-power load types.

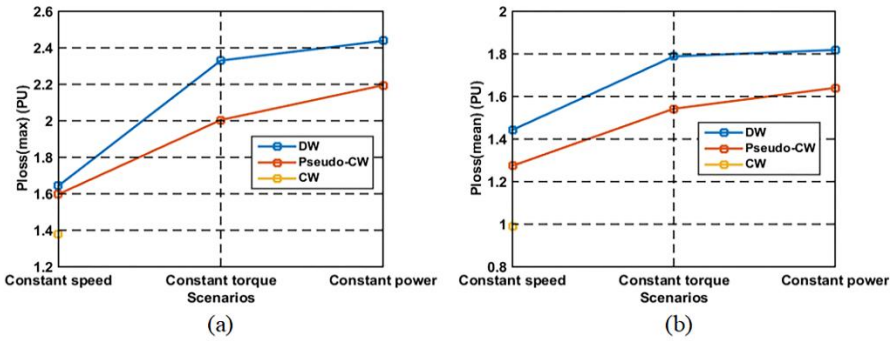

Figure 10. FEA results for (a) minimum and (b) average power losses of 6PIMs with DW, CW, and pseudo-CW.

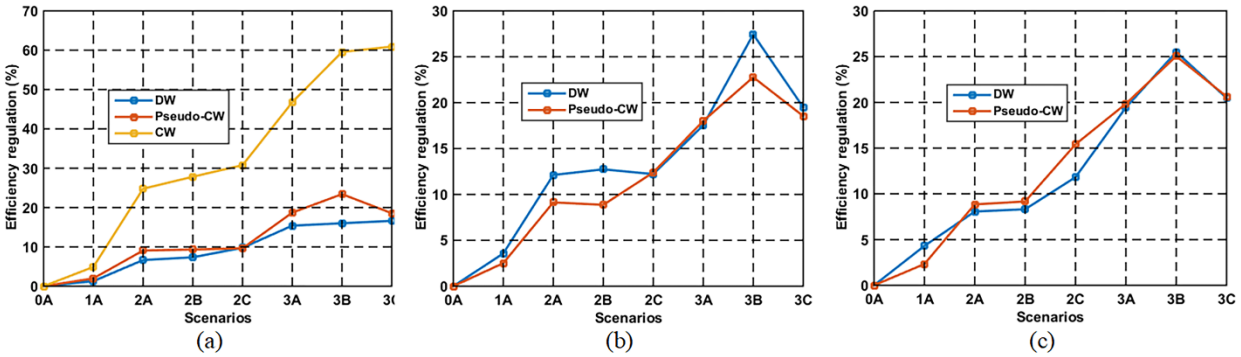

Figure 11. Efficiency of 6PIM under different fault scenarios: (a) Constant-speed (b) Constant-torque (c) Constant-power load types.

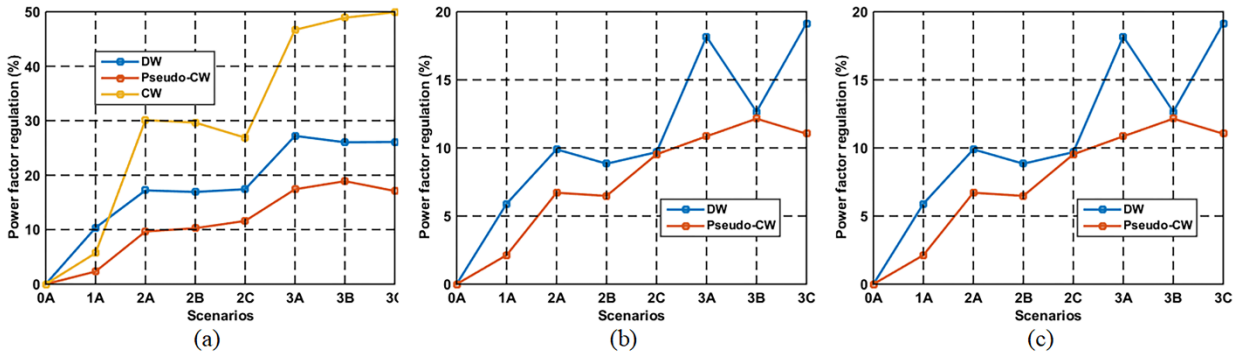

Figure 12. Power factor of 6PIM under different fault scenarios: (a) Constant-speed (b) Constant-torque (c) Constant-power load types.

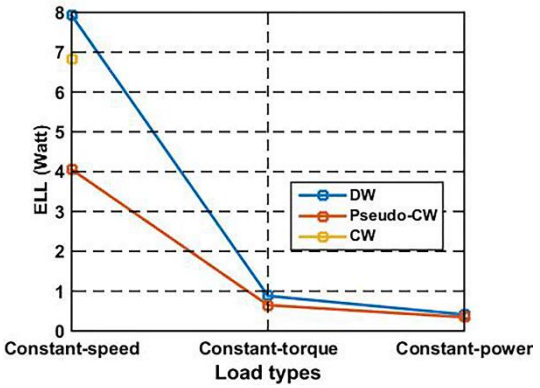

Figure 13. ELL of 6PIM under different load conditions.

Table 1. Baseline motor parameters.

Quantity	Unit	Measured Value
External stator diameter	mm	79.5
Internal stator diameter	mm	41.8
Active core length	mm	45.7
Air gap thickness	mm	0.4
Stator slot number	-	24
Stator slot area	mm^2	12.9
Rotor slot number	-	18
Rotor bar area	mm^2	16.8
External end-ring diameter	mm	39.5
Internal end-ring diameter	mm	27
End-ring thickness	mm	7
Inertia coefficient	$kg.m^2$	4.10-4

Table 2. Performance variables of baseline motor.

Quantity	Unit	DW		CW	Pseudo-CW	
		FEA	Exp [6]	FEA	FEA	Exp [6]
Phase voltage	V	14	14	5.1	10.7	10.7
Turns per slot	-	27	27	28	40	40
Rated current	A	1.82	1.78	1.77	1.78	1.8
No-load current	A	1.45	1.41	1.69	1.62	1.63

Rated speed	rpm	2822	2820	2820	2820	2820
Rated torque	N.m.	0.3	0.3	0.069	0.151	0.16
Power factor	p.u.	0.722	-	0.541	0.651	0.644
Efficiency	%	80.2	-	69.5	60.1	63.6

Table 3. FEA results for phase-to-phase inductances

(a) Distributed winding

Phases	Phase A_1	Phase A_2	Phase B_1	Phase B_2	Phase C_1	Phase C_2
Phase A_1	1	0.4285	0.4285	0.8931	0.4285	0.4285
Phase A_2	0.4285	1	0.4285	0.4285	0.8931	0.4285
Phase B_1	0.4285	0.4285	1	0.4285	0.4285	0.8931
Phase B_2	0.8931	0.4285	0.4285	1	0.4285	0.4285
Phase C_1	0.4285	0.8931	0.4285	0.4285	1	0.4285
Phase C_2	0.4285	0.4285	0.8931	0.4285	0.4285	1

(b) Conventional concentrated winding

Phases	Phase A_1	Phase A_2	Phase B_1	Phase B_2	Phase C_1	Phase C_2
Phase A_1	1	0.0169	0.0169	0.0341	0.0169	0.0169
Phase A_2	0.0169	1	0.0169	0.0169	0.0341	0.0169
Phase B_1	0.0169	0.0169	1	0.0169	0.0169	0.0341
Phase B_2	0.0341	0.0169	0.0169	1	0.0169	0.0169
Phase C_1	0.0169	0.0341	0.0169	0.0169	1	0.0169
Phase C_2	0.0169	0.0169	0.0341	0.0169	0.0169	1

(c) Pseudo-concentrated winding

Phases	Phase A_1	Phase A_2	Phase B_1	Phase B_2	Phase C_1	Phase C_2
Phase A_1	1	0.2331	0.2331	0.9659	0.2331	0.2331
Phase A_2	0.2331	1	0.2331	0.2331	0.9659	0.2331
Phase B_1	0.2331	0.2331	1	0.2331	0.2331	0.9659
Phase B_2	0.9659	0.2331	0.2331	1	0.2331	0.2331
Phase C_1	0.2331	0.9659	0.2331	0.2331	1	0.2331
Phase C_2	0.2331	0.2331	0.9659	0.2331	0.2331	1

Table 4. Different fault scenarios for symmetrical six-phase induction motor.

OCF		scenarios	phase fault
Number of OCFs	Faults		
0 OCF	0Ph	0A	-
1 OCF	1Ph	1A	A_1
2 OCFs	A2Ph	2A	A_1-A_2
	NA2Ph	2B	A_1-B_1
	NA2Ph	2C	A_1-B_2
3 OCFs	A3Ph	3A	A_1-A_2-B_1
	NA3Ph	3B	A_1-A_2-B_2
	NA3Ph	3C	A_1-B_1-C_1

Table 5. FEA results for performance of 6PIM equipped with DW

(a) Constant-speed

Scenarios \ Parameter	Vph	I_{A1}	I_{A2}	I_{B1}	I_{B2}	I_{C1}	I_{C2}	Torque		Speed	Copper loss	P_{LL}	Power factor	P out	Efficiency
								Full load torque	Torque ripple						
0A	14	1.76	1.76	1.76	1.76	1.76	1.76	0.3	26%	2822	18.6	0.00	0.81	88.66	74%
1A	14	0	2.12	2.14	2.24	2	2.02	0.29	56%	2822	22.2	2.96	0.73	85.70	73%
2A	14	0	0	2.47	2.68	2.61	2.29	0.25	70%	2822	25.3	8.66	0.67	80.00	69%
2B	14	0	2.36	0	2.67	2.41	2.58	0.26	74%	2822	25.2	9.26	0.67	79.40	68%
2C	14	0	2.51	2.49	0	2.54	2.51	0.26	120%	2822	25.3	11.66	0.67	77.00	67%
3A	14	0	0	0	3.28	3.24	3.05	0.238	30%	2822	30.6	18.66	0.59	70.00	63%
3B	14	0	0	3.04	0	3.36	3.01	0.232	145%	2822	29.6	19.16	0.60	69.50	62%
3C	14	0	3.13	0	3.16	0	3.14	0.231	26%	2822	29.6	19.66	0.60	69.00	62%

(b) Constant-torque

Scenarios \ Parameter	Vph	I_{A1}	I_{A2}	I_{B1}	I_{B2}	I_{C1}	I_{C2}	Torque		Speed	Copper loss	P_{LL}	Power factor	P out	Efficiency
								Full load torque	Torque ripple						
0A	14	1.76	1.76	1.76	1.76	1.76	1.76	0.3	25%	2822	18.6	0.00	0.81	88.66	74%
1A	14	0	2.12	2.1	2.24	2.1	2.02	0.3	60%	2812	22.4	0.31	0.76	88.34	71%
2A	14	0	0	2.67	2.82	2.8	2.46	0.3	64%	2790	29.0	1.01	0.73	87.65	65%
2B	14	0	2.54	0	2.82	2.6	2.75	0.3	68%	2791	28.7	0.97	0.74	87.68	64%
2C	14	0	2.68	2.67	0	2.74	2.65	0.3	112%	2787	28.8	1.10	0.73	87.56	65%
3A	14	0	0	0	3.74	3.72	3.52	0.3	30%	2754	40.2	2.14	0.65	86.52	61%
3B	14	0	0	3.67	0	4.1	3.61	0.3	134%	2730	43.3	2.89	0.71	85.77	54%
3C	14	0	3.7	0	3.74	0	3.72	0.3	22%	2745	41.5	2.42	0.66	86.24	59%

(c) Constant-power

Scenarios \ Parameter	Vph	I_{A1}	I_{A2}	I_{B1}	I_{B2}	I_{C1}	I_{C2}	Torque		Speed	Copper loss	P_{LL}	Power factor	P out	Efficiency
								Full load torque	Torque ripple						
0A	14	1.79	1.79	1.79	1.79	1.79	1.79	0.3	26%	2822	19	0.00	0.80	88.66	74%
1A	14	0	2.12	2.12	2.25	2.08	2.01	0.3	56%	2813	22	0.28	0.77	88.37	71%
2A	14	0	0	2.62	2.81	2.81	2.46	0.302	68%	2792	29	0.36	0.71	88.30	68%
2B	14	0	2.51	0	2.89	2.65	2.76	0.305	65%	2757	29	0.60	0.70	88.06	68%
2C	14	0	2.81	2.72	0	2.77	2.7	0.308	120%	2747	30	0.05	0.72	88.60	65%
3A	14	0	0	0	3.87	3.86	3.65	0.311	29%	2705	43	0.56	0.66	88.10	60%
3B	14	0	0	3.8	0	4.33	3.7	0.311	128%	2670	47	1.70	0.67	86.96	55%
3C	14	0	3.82	0	3.82	0	3.85	0.312	24%	2670	44	1.70	0.65	86.96	59%

Table 6. FEA results for performance of 6PIM equipped CW

Constant-speed

Scenarios \ Parameter	Vph	Ia_1	Ia_2	Ib_1	Ib_2	Ic_1	Ic_2	Torque		Speed	Copper loss	P_{LL}	Power factor	P out	Efficiency
								Full load torque	Torque ripple						
0A	5.1	1.77	1.77	1.77	1.77	1.77	1.77	0.069	110%	2820	9.40	0.00	0.63	20.38	61%
1A	5.1	0	2.4	1.85	1.26	2.41	1.88	0.064	180%	2820	10.06	1.48	0.60	18.90	58%
2A	5.1	0	0	2.5	1.21	1.68	2.58	0.034	217%	2820	8.26	10.34	0.49	10.04	46%
2B	5.1	0	2.58	0	1.7	2.44	1.41	0.036	208%	2820	9.92	9.75	0.50	10.63	44%

2C	5.1	0	2.9	2.15	0	2.88	2.14	0.041	280%	2820	12.95	0.30	0.52	20.08	42%
3A	5.1	0	0	0	1.86	1.56	1.99	0.016	600%	2820	6.27	15.65	0.40	4.72	33%
3B	5.1	0	0	2.7	0	1.91	2.68	0.014	950%	2820	9.06	16.24	0.44	4.13	25%
3C	5.1	0	1.99	0	2	0	1.98	0.013	760%	2820	8.70	16.54	0.38	3.84	24%

Table 7. FEA results for performance of 6PIM equipped Pseudo-CW: (a) Constant-speed (b) Constant-torque (c) Constant-power

(a) Constant-speed

Parameter / Scenarios	Vph	Ia_1	Ia_2	Ib_1	Ib_2	Ic_1	Ic_2	Torque		Speed	Copper loss	P_{LL}	Power factor	P out	Efficiency
								Full load torque	Torque ripple						
0A	10.7	1.78	1.78	1.78	1.78	1.78	1.78	0.151	30%	2820	19	0.00	0.62	44.59	63%
1A	10.7	0	2.01	1.80	2.29	2.03	1.80	0.148	80%	2820	20	0.98	0.61	43.61	61%
2A	10.7	0	0	2.16	2.41	2.71	2.19	0.135	80%	2820	23	4.67	0.56	39.93	57%
2B	10.7	0	2.13	0	2.69	2.20	2.39	0.133	78%	2820	22	5.28	0.56	39.31	57%
2C	10.7	0	2.63	1.94	0	2.59	2.00	0.128	150%	2820	21	6.82	0.55	37.78	57%
3A	10.7	0	0	0	2.94	2.97	3.00	0.120	28%	2820	26	9.27	0.51	35.32	51%
3B	10.7	0	0	2.96	0	3.12	2.93	0.119	148%	2820	30	9.58	0.50	35.01	48%
3C	10.7	0	2.96	0	2.99	0	3.00	0.121	27%	2820	27	8.97	0.52	35.63	51%

(b) Constant-torque

Parameter / Scenarios	Vph	Ia_1	Ia_2	Ib_1	Ib_2	Ic_1	Ic_2	Torque		Speed	Copper loss	P_{LL}	Power factor	P out	Efficiency
								Full load torque	Torque ripple						
0A	10.7	1.78	1.78	1.78	1.78	1.78	1.78	0.151	30%	2820	19	0.00	0.62	44.59	63%
1A	10.7	0	2.06	1.84	2.32	2.10	1.82	0.151	80%	2811	21	0.14	0.61	44.46	61%
2A	10.7	0	0	2.31	2.57	2.89	2.32	0.151	80%	2775	26	0.71	0.58	43.88	57%
2B	10.7	0	2.31	0	2.89	2.29	2.57	0.151	78%	2783	25	0.58	0.58	44.01	57%
2C	10.7	0	3.02	2.25	0	3.01	2.28	0.151	150%	2735	28	1.34	0.56	43.25	55%
3A	10.7	0	0	0	3.32	3.33	3.33	0.151	28%	2723	33	1.54	0.55	43.06	51%
3B	10.7	0	0	3.52	0	3.71	3.47	0.151	141%	2709	38	1.76	0.55	42.83	48%
3C	10.7	0	3.32	0	3.36	0	3.37	0.151	27%	2720	34	1.58	0.55	43.01	51%

(c) Constant-power

Parameter / Scenarios	Vph	Ia_1	Ia_2	Ib_1	Ib_2	Ic_1	Ic_2	Torque		Speed	Copper loss	P_{LL}	Power factor	P out	Efficiency
								Full load torque	Torque ripple						
0A	10.7	1.78	1.78	1.78	1.78	1.78	1.78	0.151	26%	2820	19	0.00	0.62	44.59	63%
1A	10.7	0	2.05	1.84	2.32	2.06	1.81	0.151	64%	2802	21	0.28	0.61	44.31	61%
2A	10.7	0	0	2.33	2.57	2.86	2.34	0.153	70%	2760	26	0.37	0.58	44.22	57%
2B	10.7	0	2.34	0	2.90	2.33	2.57	0.153	70%	2760	26	0.37	0.58	44.22	57%
2C	10.7	0	3.19	2.38	0	3.19	2.40	0.16	138%	2650	32	0.19	0.57	44.40	53%
3A	10.7	0	0	0	3.48	3.46	3.48	0.156	24%	2700	36	0.48	0.56	44.11	50%
3B	10.7	0	0	3.71	0	3.90	3.58	0.155	136%	2690	42	0.93	0.55	43.66	47%
3C	10.7	0	3.47	0	3.52	0	3.50	0.155	22%	2675	37	0.89	0.55	43.70	50%

Biographies:

Mehdi Alemi-Rostami was born in Behashahr, Iran, in 1980. He received the B.Sc. degree from Gilan University, Gilan, Iran, in 1998, and the M.S. and Ph.D. degrees from Iran Unicersity of Science and Technology, Tehran, Iran, in 2000 and 2011, respectively, all in power electronics. He is currently an Assistant Professor with the Khayam Research Institute (KRI), Ministry of Science, Research, and Technology, Tehran, Iran.

Ghasem Rezazadeh was born in Freydoonkenar, Iran, in 1990. He received the B.S. degree in electrical engineering from Shahid Beheshti University in 2012. In 2014, he received his M.Sc. degree from Sharif University of Technology, Tehran, Iran. He Received his Ph.D. degree in a co-supervision in between Sharif University of Technology and the University of Picardie "Jules Verne", Amiens, France. His research interests include electrical machine design, modeling and drive.

Farzad Tahami received the B.S. degree in electrical engineering from Ferdowsi University of Mashhad, Mashhad, Iran, in 1991, and the M.S. and Ph.D. degrees in electrical engineering from the University of Tehran, Tehran, Iran, in 1993 and 2003, respectively. From 1991 to 2004, he was with R&D department of Jovain Electrical Machines Corporation (JEMCO), Iran. In 2004, he joined Sharif University of Technology, Tehran, Iran, where he is currently an Associate Professor. Since 2007, he has been the Chairman of the technical committee of rotating machinery, The Iranian National Electrotechnical Committee (INEC). Dr. Tahami is a Member of the Board of Directors and the Chairman of the education committee of the Power Electronics Society of Iran (PESI). His current research interests include electric motor drives, modeling and control of power electronic converters, soft switching, resonant converters, and wireless power transfer.

Hamid Reza Akbari-Resketi was born in Sari, Iran, in 1992. He received the M.Sc. degree in electrical power engineering from the Babol Noshirvani University of Technology, Babol, Iran in 2019. His research interests include design, simulation, optimization, control, and performance analysis of electrical machines.